CREEP CLOSURE OF SALT CAVERNS

IN THE

STRATEGIC PETROLEUM RESERVE

Grant S. Heffelfinger
Underground Storage Technology Division 6257
Sandia National Laboratories
Albuquerque, New Mexico 87185

ABSTRACT

The U.S. Department of Energy maintains the Strategic Petroleum Reserve (SPR), a 750-million barrel crude oil reserve stored in caverns leached in Gulf Coast salt domes. Typical SPR caverns have been investigated with a simplified creep closure model in an effort to predict the long-term effects of creep closure on the caverns as well as to ascertain the relationships between lost volume and operational procedure. In particular, the effects of operating the caverns at a higher wellhead pressure, in order to mitigate volume loss, were investigated. As expected, higher volume losses were found for deeper caverns and caverns operated at lower wellhead pressure. In addition, the reduction in volume lost for a given increase in wellhead pressure was found to increase nonlinearly with increasing cavern depth. The distribution of the volume loss was also calculated. This distribution was found to be only slightly dependent on cavern depth, with 80 to 90% of the volume loss occurring in the bottom 30% of the caverns. Finally, the results from *two* different temperature approximations were compared. As most engineering calculations of creep assume a constant, average temperature throughout the oil and salt, this temperature profile was compared to one that was linear in the axial direction while invariant in the radial and **time** dimensions. The results of the two methods of approximating temperature, for volume loss of caverns operated for 30 years at 41.4 bar (600 psia), were found to deviate nonlinearly with cavern depth. The volume loss predicted by the average temperature model was up to 35% less than that predicted by the linear temperature profile.

ACKNOWLEDGEMENTS

INTRODUCTION

Underground salt domes have been studied for a variety of uses including the mining of salt, storage of petroleum products and radioactive and chemical waste, and compressed air energy storage. Salt dome utilization generally requires the formation of cavities in the dome itself. Once formed, these cavities begin to creep closed due to the lithostatic stress on the cavity walls and the plasticity of the salt.

The creep closure of these salt dome cavities is of particular interest to the U.S. Department of Energy which maintains the Strategic Petroleum Reserve (SPR). This reserve contains over 750-million barrels of crude oil stored underground in salt domes along the Gulf Coast. These underground cavities range from a converted salt mine in the Weeks Island dome, to the cylindrical Phase II/III caverns in other domes leached specifically for crude oil storage.

An idealized Phase II/III cavern is shown in Figure 1. These caverns are generally 610 m (2000 ft) on axis with a radius of 30.5 m (100 ft). A cased well with a hanging string extends from the surface to the cavern. As the cavern creeps inward due to the lithostatic pressure (which exceeds the cavern pressure), the cavern pressure rises and is controlled by removing brine from the cavern thus preventing the pressure at the casing seat from approaching its design limit. The oil is withdrawn by injecting fresh water into the brine region through the hanging string, floating the oil out of the cavern through the **annulus** between the hanging string and the well. Because fresh water is used for the drawdown, additional volume is leached during drawdown.

PREVIOUS WORK

In an effort to predict the long-term effects of creep closure on the salt dome cavities, as well as to ascertain the relationships between lost volume and operational procedure, a number of studies have been conducted. The first step towards mathematically characterizing creep closure of salt dome cavities is to determine the nature of the salt itself. Once the salt's creeping response to pressure has been represented mathematically, long-term creep on cavities can be modelled.

Numerous studies consisting primarily of laboratory measurements have demonstrated that creep in rock salt occurs in three different regimes: a transient phase, followed by a steady state phase, and finally a rupture phase. The steady state regime, where the bulk of the salt response is concentrated, is often **modelled** by a power law:

$$\dot{\gamma}_s = C \exp\left(\frac{-Q}{R_g T}\right) \left(\frac{\tau}{\mu}\right)^n \tag{1}$$

Typical SPR Cavern

$z_{surf} =$ **0** m
(0 ft)

$z_t =$ **610** m
(2000 ft)

$z_i =$ **1143** m
(3750 ft)

$z_b =$ **1219** m
(4000 ft)

Overburden

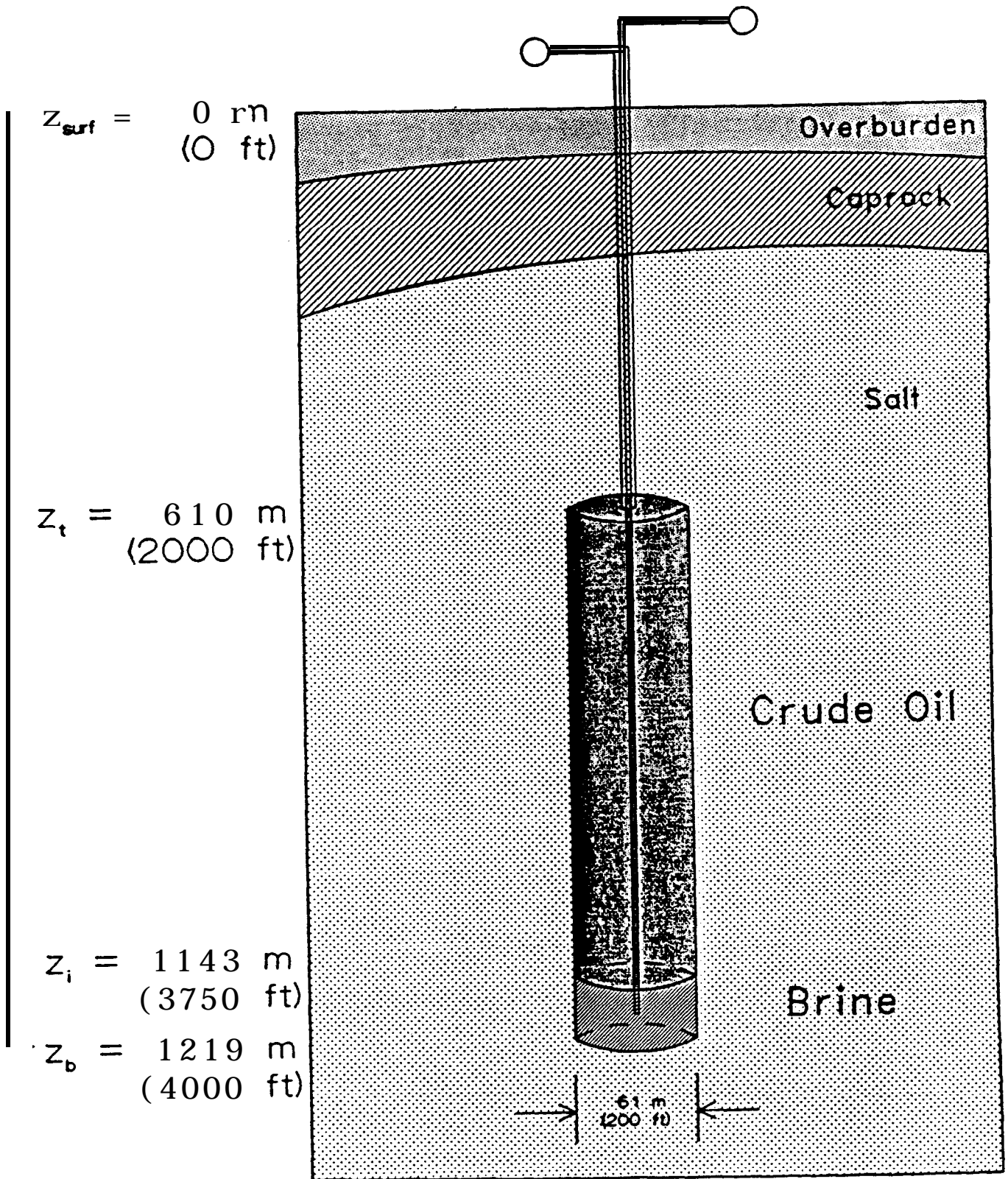Caprock

Salt

Crude Oil

Brine

61 m
(200 ft)

Figure 1. Typical SPR cavern, 610 m - 1219 m **(2000** ft - 4000 ft), with **wellhead** pressure maintained at or near 41.4 bar (600 psia) and with the initial oil/brine interface at a depth of 76 m (250 ft) above the cavern floor.

In this equation, $\dot{\gamma}_s$ represents the steady state creep rate, while C and Q are constants, R_g is the universal gas constant, T is temperature, μ is an average shear modulus, τ denotes the effective stress (a scalar measure of the deviatoric stress components at a point in the salt), and n is the steady state creep exponent, usually taken to be between 3.5 and 5.5. Several reviews of the work characterizing salt creep via laboratory and in situ measurements have been published.[1,2,3,4,5] By incorporating salt creep equations, such as the power law in computer codes, creep closure calculations can be performed for a wide variety of salt dome cavities. Past studies have generally employed finite element analysis while approximating the salt response with a steady state model, neglecting the transient response. Several authors have quantified this approximation. For example, Morgan et al.[6] have found that including transient creep does not significantly affect the agreement between in situ measurements and calculations of creep closure.

The caverns modelled with finite element analysis have varied in size and shape. Anderson[7] performed a finite element analysis of a spherical cavity in a half space. Representing the salt creep with the steady state power law model, Anderson investigated the effects of the temperature field in the dome, the depth-to-radius ratio of the cavity, and the pressure in the cavity (taken to be constant) on volume loss and creep rate. Van Sambeek[8] used finite element analysis as well as an approximate analytical solution to investigate the pressure evolution and rate of creep closure for plugged and abandoned solution (brine-filled) wells. The compressibility of the brine was taken to be constant while temperature, well pressure, and lithostatic pressure were modelled as linear functions of depth. Agreement between the finite element and analytical methods was found to be dependent on cavern shape. In a similar study, Preece et al.[9] employed finite element analysis to calculate creep closure in brine-filled boreholes in the Big Hill SPR salt dome. Again, the compressibility of the brine was taken to be constant while temperature, well pressure, and lithostatic pressure were modelled as linear functions of depth. The results of these calculations, radial displacements and wellhead pressures, were compared to field measurements. The measured values of these parameters were found to exceed the calculated values by a factor of 2 to 2.5. In another finite element analysis, Preece and Foley[10] calculated volume loss due to creep closure while investigating the relationship between cavern spacing and structural safety. This work employed the steady state power law with an allowance for fracturing and was conducted for the designated thirty-year lifespan of SPR caverns. In order to include the effects of drawdown leaching, the cavern shape was modified every five years by simulating a drawdown. This was facilitated by a solution mining code developed by Russo.[11] Cavern spacing was also investigated in a similar finite element study by Ratigan and DeVries.[12] Although the effects of cavern drawdown were not included in this study, Ratigan and DeVries did investigate the relevance of cavern operation parameters, wellhead pressure in particular, on potential cavern collapse due to creep. Fischer[13] investigated creep effects on batteries of caverns in a single dome. In particular, the results of an axisymmetric method of "capturing three-dimensional effects within the constraints of a two-

dimensional analysis" were compared to those of finite element analysis. The pseudo-three-dimensional axisymetric method predicted less creep in the caverns. This is due largely to the presence of the cavern roof and floor material in the three-dimensional finite element analysis, which has the effect of "slowing" radial creep in these regions.

Finally, **Todd**[14] evaluated creep closure for SPR Phase II/III caverns at different **wellhead** pressures. By assuming a cavern pressure which varied linearly with depth, for a 610 m (2000 ft) cavern with a roof depth of 610 m (2000 **ft),** filled entirely with crude oil, Todd calculated the ratio of the volume loss for caverns operated at pressures other than 41.4 bars (600 psia) to that of a cavern operated at 41.4 bars (600 psia) using a power law model with various exponents.

The current work has been conducted to address several topics: (1) the effects of cavern depth and **wellhead** pressure on creep closure, (2) the distribution of volume loss with depth, and (3) the effect of the temperature approximation on the results of creep closure calculations. Moreover, these topics have been addressed through the use of a simplified creep model capable of performing the same sort of **calulations** typically carried out by the finite element method. Other topics which cannot be addressed with the finite element method but are easily explored with this model, such as the evolution of the oil/brine interface depth with time and the effects of an oil leak on the creep closure, **wellhead** pressure, and interface depth, have been discussed elsewhere.15

MODEL

The model used in this work considers radial creep only, an approximation which improves with increasing aspect ratio (length/diameter). Throughout this work, this ratio is 10. The program is initialized by a right circular cylinder radial profile. In addition, an initial **wellhead** pressure $P_w(t=0)$, and an initial interface depth, $z_i(t=0)$ are required. Because the equations of state for both brine and crude are included in the model (and thus each fluid's compressibility), P_w and z_i can be calculated (by iteration) from the equations governing cavern creep. Thus, it is possible to calculate the variation in P_w, z_i, and r(z) with time.   The motivation in writing the program to allow P_w to change with time is that this approach allows the only measurable parameters for actual caverns, P,, z_i, and the rate of fluid removal, to be related to the creep rate, complimenting previous finite element studies of creep closure for SPR caverns which have generally employed the following assumptions: constant or nearly constant P,, a single fluid i.e. no interface, and no fluid removal. Assuming constant Pw precludes the necessessity of allowing for the elastic (time-independent) response of the cavern. Although all of the results presented in this paper assume constant Pw, any application of the model which allows Pw to vary with time would require either an allowance for an elastic response, or evidence that its contribution is negligible. Such applications might provide information concerning the time-dependent behavior of P_w and z_i

which is particularly useful when examining real cavern data, $P,(t)$ and $z_i(t)$, in an effort to detect cavern leaks.

Due to the nature of SPR caverns, the actual temperature profile of the salt near SPR caverns is unknown. Although the temperature profile in the salt dome itself can be measured, once a cavern is filled this profile begins to vary as a function time and the distance from the cavern axis. This is a direct result of introducing oil into the cavern at a temperature below that of the salt. Convective heat transfer between the salt and the oil changes the temperature gradient in the salt near the cavern. As no attempts have been made to measure the temperature gradient in the salt near the cavern, the actual salt temperature profile is unknown. Most authors employ an average temperature, based on temperature logs of SPR caverns which show the temperature of the oil to vary as little as **0.0036°C/m (0.002°F/ft)**. Numerical work has been done to estimate the rate of circulation in SPR caverns[16] and the long term effects of the lower initial temperature of oil on the temperature profile in the surrounding salt[17]. In particular, Tomasko[17] found that nine years after filling an SPR cavern, the effect of the lower oil fill temperature extended some 0.9 cavern diameters from the cavern wall into the salt, with the salt nearest the cavern obviously affected the most. The temperature extending from the cavern wall to 0.2 diameters into the salt was calculated to be constant and equal to a value **8.3°C** (15°F) higher than that of the stored oil. From 0.2 to 0.9 cavern diameters from the wall into the salt, the radial temperature profile at a given depth increased from its constant value at 0.2 diameters to the lithostatic value at 0.9 cavern diameters. Beyond 0.9 cavern diameters, the salt exhibited its original lithostatic temperature gradient. The most accurate model of the temperature profile in the salt surrounding an SPR cavern would therefore be at least two dimensional and time dependent in a manner consistent with the thermal equilibrium process ongoing between the stored oil and the salt. The two extremes examined here, linear variation with depth and constant average temperature, represent bounds on either side of the actual temperature field.

The derivation of the equations governing the model begins with a force balance on a fluid element:

$$\frac{dP}{dz} = \rho g \tag{2}$$

where P is the pressure, z the axial coordinate, ρ the density, and g the gravitational constant. This relationship holds in both the crude and brine regions. Thus if the axial coordinate increases positively with depth and is zeroed at the surface,

$$\frac{dP(z)}{dz} = \rho_C g \qquad 0 \le z \le z_i \qquad (3)$$

$$\frac{dP(z)}{dz} = \rho_B g \qquad z_i \le z \le z_b \qquad (4)$$

where the subscripts C and B denote crude oil and brine, respectively. The axial coordinates of the top and bottom of the cavern and the crude/brine interface depth are denoted z_t, z_b, and z_i respectively.

In order to integrate equations (3) and (4), expressions for ρ_c and ρ_B are required. An equation of state for crude oil can be found in the Petroleum Production Handbook[18] and rearranged in the form

$$\rho_C = \rho_C^o(T) \left\{ 1 - c_C^T T + C_i(T) \, P \right\} \qquad (5)$$

with

$$\rho_C^o(T) = \rho_{H_2O}(T) \left\{ 1.00009456 + 0.16595 \right\} \frac{g}{cm^3} \qquad (6)$$

$$c_-^T = \frac{5.7627 \times 10^{-4}}{c \ 1.00009456 + 0.16595} \frac{1}{K} \qquad (7)$$

$$C_{Pc}(T) = \left\{ \frac{.018 \ 1.00009456 \ T/K + 6.436 \ 0.16595 + 3.6}{} \right\} \underline{1.45 \ bar \times 10^{-5}} \qquad (8)$$

where T denotes temperature (in K) and δ is the crude oil specific gravity, taken to be 0.876 throughout this work. For computional simplicity, $\rho_c^o(T)$ is taken to be 1.0296 g/cm^3 throughout this work (the variation with temperature of this parameter, 0.05% change per degree K, has been neglected). In the analysis that follows, it will be referred to simply as ρ_C^o. The value of this parameter was obtained by assuming a nominal cavern temperature of 323 K (121°F), the temperature at a depth of 914 m (3000 ft) (from equation (15)). The value of the parameter $\rho_{H_2O}^o(323 \ K)$, taken to be 0.98807 g/cm^3, was obtained from the Handbook of Chemistry and Physics[19]. A similar equation of state has been developed for saturated brine (see Appendix A):

$$\rho_B = \rho_B^o \left\{ 1 - c_B^T T + c_B^{T^2} T^2 + c_B^{T^3} T^3 + c_B^P P_B \right\} \qquad (9)$$

where

$$\rho_B^o = 2.0149 \text{ g/cm}^3 \tag{10}$$

$$c_B^T = \frac{8.4868 \times 10^{-9}}{K} \tag{11}$$

$$c_B^{T^2} = \frac{8.933 + 10^{-6}}{K^2} \tag{12}$$

$$c_B^{T^3} = \frac{-3.272 \times 10^{-3}}{K^3} \tag{13}$$

$$c_B^P = \frac{2.498 \times 10^{-5}}{\text{bar}} \tag{14}$$

Two temperature profiles were used in this work: an axially linear, radially and time invariant profile, and an average temperature profile. The expression,

$$T = m_T z + b_T \tag{15}$$

was used to model both. For the linear temperature profile, the parameters m_T and b_T were taken to be 0.0255 K/m (0.014 °F/ft) and 299.44 K respectively. Using these parameters for a cavern with z_t = 610 m (2000 ft) and z_b = 4000, the temperature at the top of the cavern is 315 K (107°F) while that at the bottom is 330.6 K (135°F). The second temperature approximation, employing an average temperature throughout the system, was accomplished by choosing m_T and b_T such that

$$T = T_{ave} = m_T z_{midpoint} + b_T \tag{16}$$

for all z, where $z_{midpoint}$ is the depth at the axial midpoint of the cavern. For example, for the above cavern, the temperature at the midpoint would be (0.0255 K/m)*914m + 299.4 K = 322.7 K. Thus, the input to the program would be 0.0 and 322.7 K for m_T and b_T, respectively. The average temperature approximation results in a difference of 14°F at the top and bottom of a 610 m (2000 ft) cavern.

The formulation of the model continues by substituting equation (15) for T in equations (5), (8), and (9). By making this substitution in equation (8), a second expression for the crude oil equation of state parameter $C_C^P(T)$ can be obtained:

$$c_C^P (T) = M z + B \tag{17}$$

where

$$M = \left| \frac{\cdot \ (0.018 \ 1/K) \ m_T}{1.00009456 + 0.16595} \right| \left| \frac{1.45 \times 10^{-5}}{bar} \right| \tag{18}$$

$$B = \left| \frac{(0018 \ 1/K) \ b_T - 6.436 + 3.6}{1.00009456 + 0.16595} \right| \left(\frac{1.45 \times 10^{-5}}{bar} \right) \tag{19}$$

Combining equations (3) and (5), a differential equation for the pressure in the crude region can be obtained.

$$\frac{dP}{dz} = \rho_C^o \left\{ 1 - C_C^T(m_T Z + b_T) + (M z + B) P \right\} g \tag{20}$$

Rearranging equation (19),

$$P' + P \left\{ -\rho_C^o g M z - \rho_C^o g B \right\}$$

$$= \rho_C^o g \left(1 - C_C^T b_{T_1} - \rho_C^o g C_C^T m_T z \right) \tag{21}$$

the standard form of a first-order linear ordinary differential equation is obtained. This can be solved by multiplying each side by an integrating factor[20] and then integrating. The integrating factor is calculated from:

$$\exp \left[\int \left\{ -\rho_C^o g M z - \rho_C^o g B \right\} dz \right]$$

$$= \exp \left[\frac{-\rho_C^o g M z^2}{2} - \rho_C^o g B z \right] \tag{22}$$

8

Multiplying each side of equation (21) by the right-hand side of equation (22) yields a further rearrangement of equation (21) which can be integrated,

$$
\frac{d}{dz} \left\{ P \exp\left[\frac{-\rho_C^o g \, M \, z^2 - \rho_C^o \, g \, B \, z}{2}\right]_I \right\}
$$

$$
= \left[\rho_C^o \, g \left(1 - C_C^T \, b_T\right) - \rho_C^o \, g \, C_C^T \, m_T \, z\right] \tag{23}
$$

$$
\left\{ \exp\left[-\frac{\rho_C^o g \, M \, z^2 - \rho_C^o \, g \, B \, z}{2}\right] \right\}
$$

If we define $P_t \equiv P_w + P_H$, where P_t is the pressure at the roof of the cavern ($z - z_t$) and P_H the hydrostatic head contribution of the oil column running from the **wellhead** to the roof of the cavern, we can integrate equation (23) with $P = P_t$ at $z - z_t$. This yields an expression for the pressure in the crude oil region as a function of depth:

$$
P_C(z) = \left| \int_{z_t}^{z} \left\{ \exp\left[\frac{-\rho_C^o \, g \, M \, z^2 - \rho_C^o \, g \, B \, z}{2}\right] \right\} \right.
$$

$$
\left\{\rho_C^o \, g \left(1 - C_C^T \, b_T\right) - \rho_C^o \, g \, C_C^T \, m_T \, z\right\} dz \; +
$$

$$
\tag{25}
$$

$$
P_t \exp\left\{\frac{-\rho_C^o \, g \, M \, z^2 - \rho_C^o \, g \, B \, z}{2}\right\}
$$

$$
\left. \Big/ \left\{\exp\left[\frac{-\rho_C^o g \, M \, z^2 - \rho_C^o \, g \, B \, z}{2}\right]\right\} \right.
$$

This equation can be simplified no further and is solved numerically in the program.

Substituting equation (9) into equation (4) and integrating in similar fashion, with $P = P_i = P_c(z = z_i)$, where P_i is the pressure at the interface depth z_i, evaluated from equation (25)), a similar expression can be obtained for the pressure in the brine region:

$$P_B(z) = -\frac{(1 + \Phi)}{c_B^P} + \rho_B^o \, g \, c_B^P \, Q(z) + \left\{ P_i + \frac{(1 + \Phi)}{c_B^P} \right.$$

$$\left. - \rho_B^o \, g \, c_B^P \, Q(z) \right\} \exp\left[(z - z_i)\rho_B^o \, g \, c_B^P \right] \tag{26}$$

where

$$\Phi = -c_B^T \, b_T + c_B^{T^2} \, b_T^2 + c_B^{T^3} \, b_T^3 \tag{27}$$

$$Q(z) = \frac{-\text{III } z^3}{\rho_B^o \, g \, c_B^P} - \left\{ \frac{3 \text{ III}}{\left(\rho_B^o \, g \, c_B^P\right)^2} + \frac{\text{II}}{\rho_B^o \, g \, c_B^P} \right\} z^2 - \left\{ \frac{6 \text{ III}}{\left(\rho_B^o \, g \, c_B^P\right)^3} \right.$$

$$\left. + \frac{2 \text{ II}}{\left(\rho_B^o \, g \, c_B^P\right)^2} + \frac{\text{I}}{\rho_B^o \, g \, c_F^I} \right\} \left\{ z + \frac{1}{\rho_B^o \, g \, c_B^P} \right\} \tag{28}$$

with

10

$$I = -c_B^T m_T + 2 c_B^{T^2} b_T m_T + 3 c_B^{T^3} b_T^2 m_T \tag{29}$$

$$II = c_B^{T^2} m_T^2 + 3 c_B^{T^3} m_T^2 b_T \tag{30}$$

$$III = c_B^{T^3} m_T^3 \tag{31}$$

Once expressions for the pressure have been obtained in both the crude and brine regions, the salt dome creep rate must be related to the cavern pressure. In an effort to develop a model which could adequately approximate cavern creep closure and run on small computers, a one-dimensional formulation using equation (1) was chosen for this study. The derivation is detailed by Van Sambeek[21] except that here we have used the initial cavern radius R to approximate the time-varying radius r. This approximation has been quantified, and is discussed more completely in Appendix B. This creep formulation is similar to that of Preece and Krieg[22]. Thus, the steady state creep equation used in this work is:

$$Ar = R\, A\, At\, \exp\left(\frac{-E}{R_g T}\right) \left\{ \frac{\left| K_{litho}\, z - P(z) \right|}{\mu} \right\}^{5.5} \tag{32}$$

where Ar is the change in radius, R the initial cavern radius, R_g the gas constant, T is a function of depth according to equation (15), and At is the time step. Throughout this work, R was taken to be 100 ft. The values of the other parameters in this equation are:

$$A = 2.43 \times 10^{29}\ /yr \tag{33}$$

$$E = 104.6\ kJ/mole \tag{34}$$
$$(25\ kcal/mole)$$

$$K_{litho} = 0.226\ bar/m \tag{35}$$
$$(1\ psia/ft)$$

$$\mu = 8.48 \times 10^4 bar \tag{36}$$
$$(1.23 \times 10^6\ psia)$$

These values are based on laboratory creep measurements of the parameters which were then adjusted to fit actual SPR cavern data. This data was

11

wellhead pressure data taken from Bryan Mound 110 during a 2 month quiet period in the cavern's operation.

As can be seen from equation (43) (Appendix B) the cavern creep, Ar, depends directly on the differential between the lithostatic pressure and the cavern pressure. The cavern pressure depends on the **wellhead** pressure, and the mass oil and brine in the cavern, denoted M_c and M_b respectively. The amount of oil in the cavern is usually kept constant while the brine is slowly bled to keep the pressure on the casing to within allowable limits. By knowing the initial masses of crude and brine as well as the initial **wellhead** pressure and interface depth, the **wellhead** pressure and interface depth can be followed in time if known amounts of brine are removed. Neglecting the mass of crude in the pipe between the surface and the top of the cavern, the initial mass of crude can be determined according to

$$M_C = \int_{z_t}^{z_i} \int_0^{2\pi} \int_0^{r(z)} \rho_C \, r' \, dr' \, d\theta \, dz \qquad (37)$$

Assuming that ρ_C is a function of only depth, equation (37) can be simplified to give

$$M_C = \int_{z_t}^{z_i} \rho_C \, \pi \, r^2(z) \, dz \qquad (38)$$

A similar expression for M_B can be obtained, again assuming that ρ_B is a function only of depth,

$$M_B = \int_{z_i}^{z_b} \rho_B \, \pi r^2(z) \, dz \qquad (39)$$

The next step in developing the model was to develop a computer algorithm which incorporates the above equations to calculate the cavern shape, pressure, and interface depth with time for varying conditions. This was accomplished with a FORTRAN program which requires as input the initial **wellhead** pressure and the initial interface depth.   In addition, the program requires an initial cavern geometry, taken to be a right circular cylinder throughout this work:

$$r(z, t = 0) = R \qquad (40)$$

12

The algorithm consists essentially of a large loop containing two subloops. The large loop begins with an an estimate of P_w and z_i at time $t = \Delta t$. While holding P_w constant, the estimate of z_i is then varied in the first of the **subloops** until equation (39) gives the current value for M_B, the mass of the brine in the cavern, to within an acceptable tolerance. The resulting z_i is then used in the second **subloop** in which P_w is varied in equation (38) until the current value for M_c is obtained, again to within acceptable limits. The large loop around the two smaller **subloops** is used to continue the iteration of P_w and z_i via the two **subloops** until they no longer **flucuate**. At this point, the radius of the cavern is updated using equation (32). It would be more accurate to reiterate P_w and z_i using the resulting $r(z)$, continuing until the two variables P_w and z_i as well as the function $r(z)$ were unchanging, but this proved to have little effect on the results. The radial function, **r(z)**, is stored in an array which contains 10,000 points. In effort to establish the minimum number of points necessary to store this function, several lower values were investigated. Ten thousand points was found to be the minimum necessary to insure accuracy. In addition, to increase the accuracy of the calculations, a **Newton-Gregory**[23] table look-up algorithm was employed when the r(z) array was called upon to supply a value for the radius at a given depth.

After selecting the appropriate values for the creep model parameters as well as the best dimensions for the r(z) array, an investigation was performed to determine an appropriate time step. The principal objective of this investigation was to determine at what value of the time step it ceased to have an effect on the results of the creep model. This naturally depended on the time scale of the model. For the 30 year'time **span,** the accepted lifespan of SPR caverns, the best time step was determined to be 0.1 years and thus is used throughout this work.

As mentioned above, actual SPR caverns are usually operated in a manner which has cavern pressure control as its main objective. As a result, standard SPR operating procedure consists of removing brine from the cavern every month or so, keeping cavern pressure more or less constant. In order to model this behavior, the program was written to maintain constant **wellhead** pressure by the removal of an appropriate amount of brine every time step.

RESULTS

Modelling creep in SPR caverns enables several different types of analyses. A qualitative understanding of the relationships between the operational variables and physical cavern response can be obtained via parametric studies. In addition, various approaches to approximating unknown physical phenomena, such as the temperature profile in the salt surrounding an SPR cavern, are easily compared. In particular, this work focuses on the relationships between the **wellhead** pressure and cavern depth (controllable parameters), and volume loss and interface movement. In addition, two different methods of modelling the temperature, using an average temperature and using a temperature profile linear in the axial

13

direction while invariant in the radial and time dimensions, are
compared.

Operating the program in the constant P_w mode, thus approximating normal
operating procedures, the effect of the operating pressure, P,, on the
volume lost due to creep and interface depth can be determined. The
extent of these effects will vary with cavern depth. As mentioned above,
throughout this work an initial cavern shape of a right circular
cylinder, with a radius of 30.5 m (100 ft) and an axial length of 610 m
(2000 ft) has been used. In all cases the initial interface depth was
set 76 m (250 ft) from the bottom of the cavern. Three primary caverns
have been modelled, a shallow cavern 457 m - 1067 m (1500 ft - 3500 ft),
a cavern at nominal depth 610 m - 1219 m (2000 ft - 4000 ft), and a deep
cavern 762 m - 1372 m (2500 ft - 4500 ft). The creep for each cavern has
been calculated at a range of **wellhead** operating pressures for the
mandated thirty-year lifetime of an SPR cavern using two different models
of the temperature in the salt dome.

The relationship between the volume loss, **wellhead** pressures, and cavern
depth can be demonstrated by plotting the percent volume loss as a
function of **wellhead** pressures for caverns at all three depths. This can
be accomplished with a single plot if the difference between the
lithostatic pressure and the cavern pressure at the cavern roof is used
as the abscissa. The data has been plotted in this fashion *in* Figure 2.
From this plot we can easily see that the percent volume loss
dramatically increases with increasing cavern depth. That is, for all
wellhead pressures (as expressed by $P_{litho}(z_t) - P_{cavern}(z_t)$) the shallow
cavern (dotted line) experiences a smaller percent volume loss throughout
its 30 year lifetime than that of the deep cavern (dashed line). In
addition, the effect of higher **wellhead** pressure on percent volume loss
is greater for deeper caverns. This is evident from the slope of the
lines in the normal operating pressure range, 34.5 bar - 48.3 bar
(500 psia - 700 psia). That is, in the normal operating range, the slope
of the line representing the deep cavern (dashed line) is much greater
than that of the shallow cavern (dotted line).

The relationship between volume loss and operating pressure can also be
plotted as a ratio, relative to a "standard cavern" as done by Todd[14].
Using as a standard a cavern 610 m - 1219 m (2000 ft - 4000 ft) deep,
operated for 30 years at P_w = 41.4 bars (600 psia), Todd calculated the
ratio of the volume loss of 610 m - 1219 m (2000 ft - 4000 ft) caverns
operated for 30 years at varying P,, to that experienced by the standard
cavern. Todd's results for a cavern 610 m - 1219 m (2000 ft - 4000 ft)
deep as well as similar results using the current model for caverns at
the three depths discussed above are plotted in Figure 3. The
temperature approximation is not a factor in a **comparision** of creep rates
for different caverns as the temperature components of the creep
equations drop out when divided. The deviation between Todd's results
and the results of the current model for the cavern 610 m - 1219 m
(2000 ft - 4000 ft) deep are likely due to an integration approximation
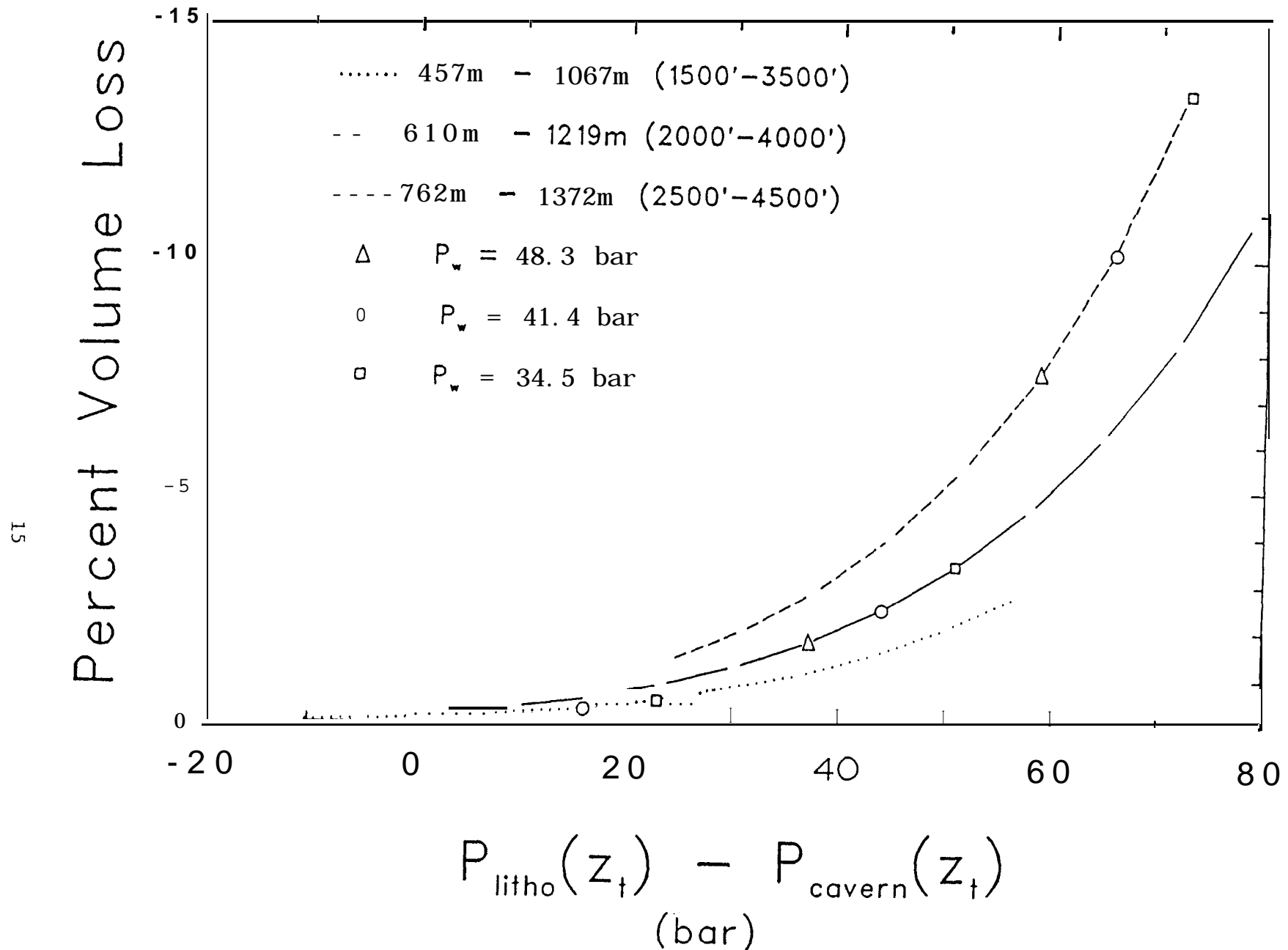Todd[14] used which degrades with decreasing P_w.

14

Figure 2. Percent volume loss plotted as a function of the difference between the lithostatic and cavern pressures at the top of the cavern, z_t, for three caverns: 457 m - 1067 m (1500 ft - 3500 ft), 610 m - 1219 m (2000 ft - 4000 ft), and 762 m - 1372 m (2500 ft - 4500 ft), operated for 30 years at a range of wellhead pressures.
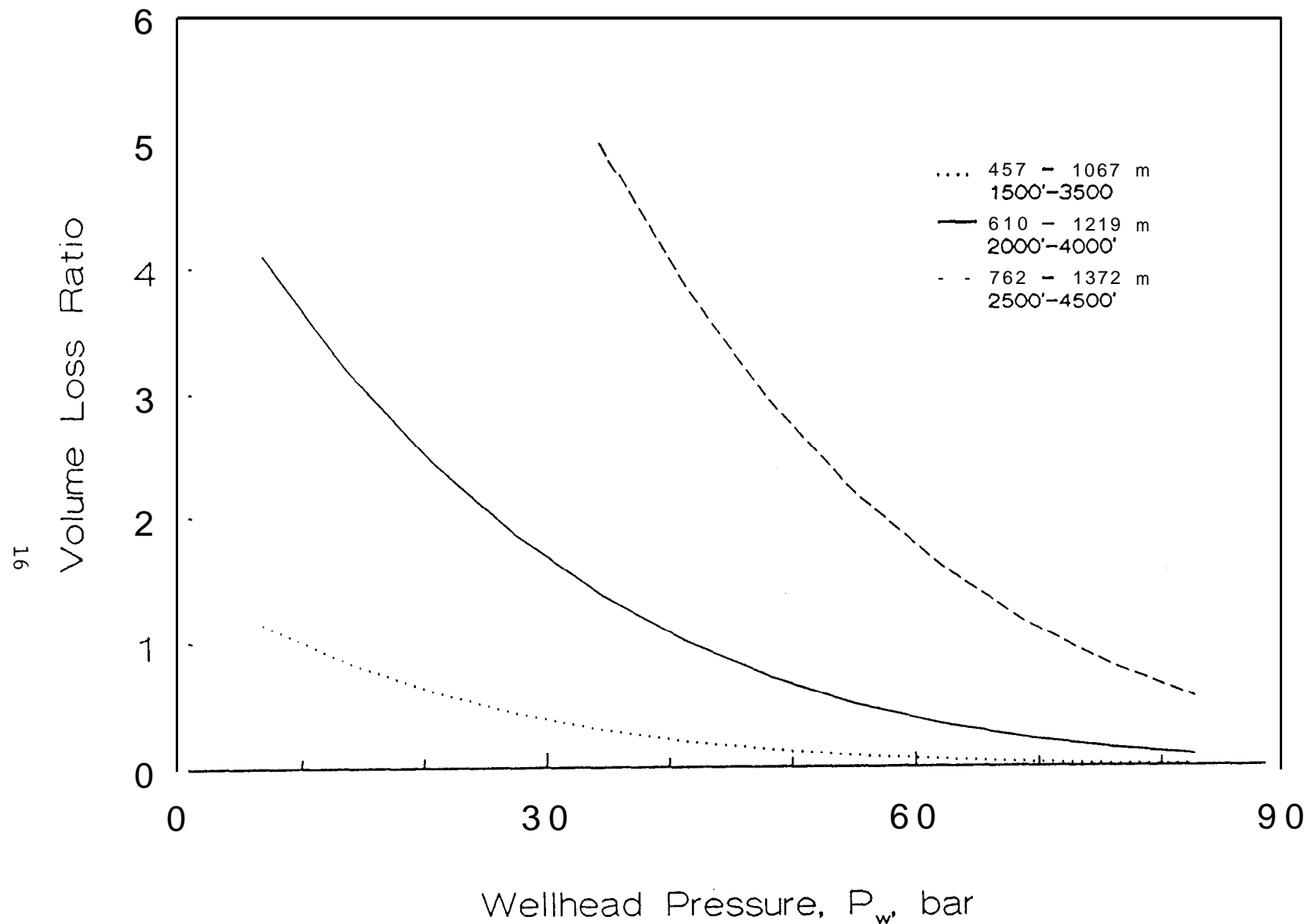
Figure 3. Volume loss calculated relative to a standard cavern, 610 m - 1219 m (2000 ft - 4000 **ft)**, operated at 41.4 bar (600 psia) for 30 years. Dotted, solid, and wide dashed lines represent volume loss for caverns of depths: 457 m - 1067 m (1500 ft - 3500 ft), 610 m - 1219 m (2000 ft - 4000 ft), and 762 m - 1372 m (2500 ft - 4500 ft), respectively, operated for 30 years at varying wellhead pressures. Todd's"' results are shown for a ca\ :rn 610 m - 1219 m (2000 Et - 4000 ft) by the line composed of narrow dashes.

While volume loss is a good indication of operational efficiency, radial profiles and interface movement indicate where and how the volume loss occurs. The radial profile at 30 years for the shallow cavern operated at four different pressures is shown in Figure 4. Normal operating **wellhead** pressure is approximately 41.4 bars (600 psia). From this figure, we immediately see that most of the creep occurs in the bottom of the cavern where the difference between cavern pressure and lithostatic pressure is the greatest. Note that the effect of the differing compressibilities of the oil and brine is unapparent from the shape of the radial profile: the creep is distributed smoothly over the entire cavern wall. It is also evident from this radial profile that higher **wellhead** pressures limit the volume loss by decreasing the radial movement of the cavern wall. Higher operating pressures offset the lithostatic pressure, resulting in a slower creep rate. In Figures 5 and 6 similar results have been plotted for the two deeper caverns. From these figures we see the influence of cavern depth on creep rate and that using higher **wellhead** pressure to minimize volume loss is more effective for deeper caverns.

Because brine withdrawal is used to maintain constant well pressure by **accomodating** volume loss, deeper caverns with higher creep rates require higher brine removal rates. Thus the level of the oil/brine interface should drop with time more dramatically for deeper caverns, subject to **wellhead** pressure. This is evident from Figures 4, 5, and 6, the radial profiles of the caverns in this study, where the interface depths at 0 and 30 years of operation have been recorded. The interface movement seen from these figures is as expected: for a given cavern, lower operating pressure requires more brine removal thus resulting in a greater interface drop. Similarly, at a given operating pressure, deeper caverns experience greater creep thus requiring greater brine removal rates, resulting in a greater interface drop.

Radial profiles can also be used to study the relationship between the creep rate and the temperature profile used in the calculation. In Figure 7, the difference in the radial profiles for the two different temperature profiles for the three caverns of varying depths has been plotted. From this figure we can see that using an average temperature not only results in a prediction of the creep rate (and therefore the volume loss) which is smaller than that predicted using the linear temperature profile, but also that the deviation between the two methods increases with increasing cavern depth.

A similar **comparision** between the two temperature models has been made in Figure 8 where the oil/brine interface depth as a function of time, calculated for the three caverns using the two different temperature profiles, has been plotted. The movement of the oil/brine interface is directly related to the brine removal rates. Therefore, calculations using the average temperature approximation will predict lower brine removal rates necessary to maintain constant pressure over the cavern's lifetime.

Perhaps the most important parameter affected by using the average temperature approximation in creep calculations is volume loss. The
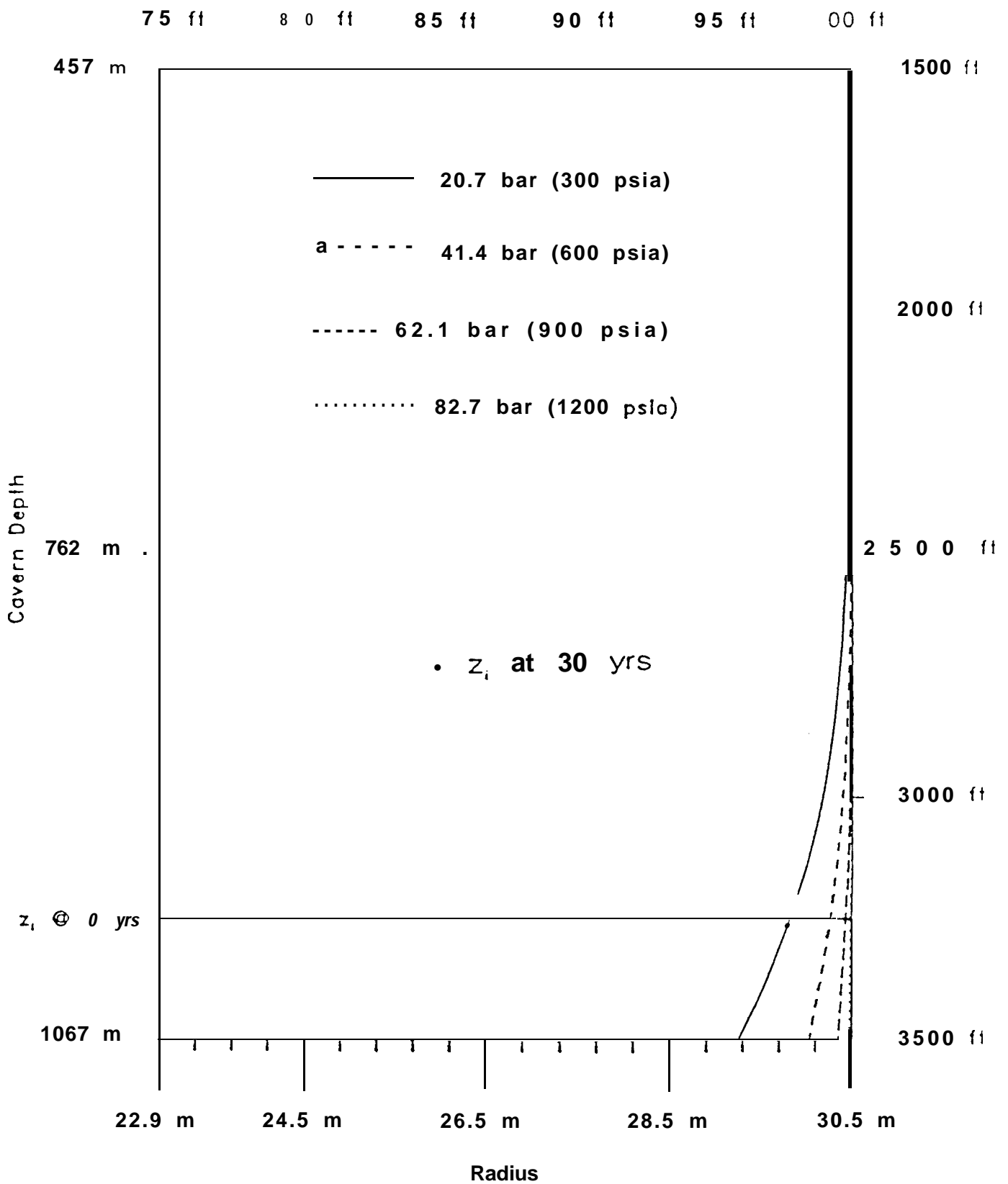
Figure 4. Radial profile, r(z), for a 457 **m** - 1067 m (1500 ft - 3500 ft) operated for 30 years at 20.7, 41.4, 62.1, and 82.7 bar (300, 600, 900, and 1200 psia). The solid horizontal line denotes the initial interface depth, 991 m (3250 ft), while the filled black circles on the radial profiles represent the interface depth at 30 years.
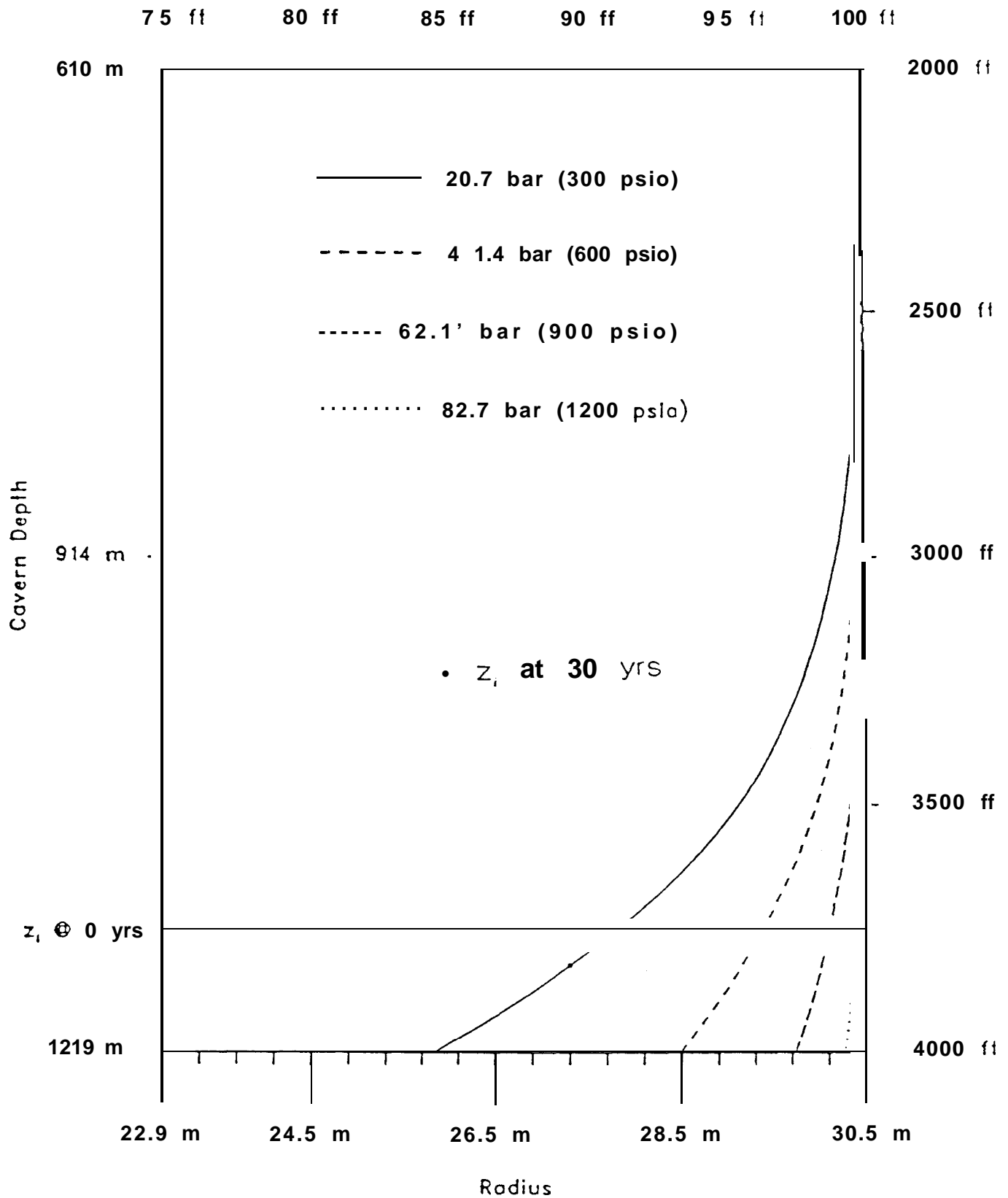
Figure 5. Radial profile, r(z), for a 610 m - 1219 m (2000 ft - 4000 ft) operated for 30 years at 20.7, 41.4, 62.1, and 82.7 bar (300, 600, 900, and 1200 psia). The solid horizontal line denotes the initial interface depth, 1143 m (3750 ft), while the filled black circles on the radial profiles represent the interface depth at 30 years.
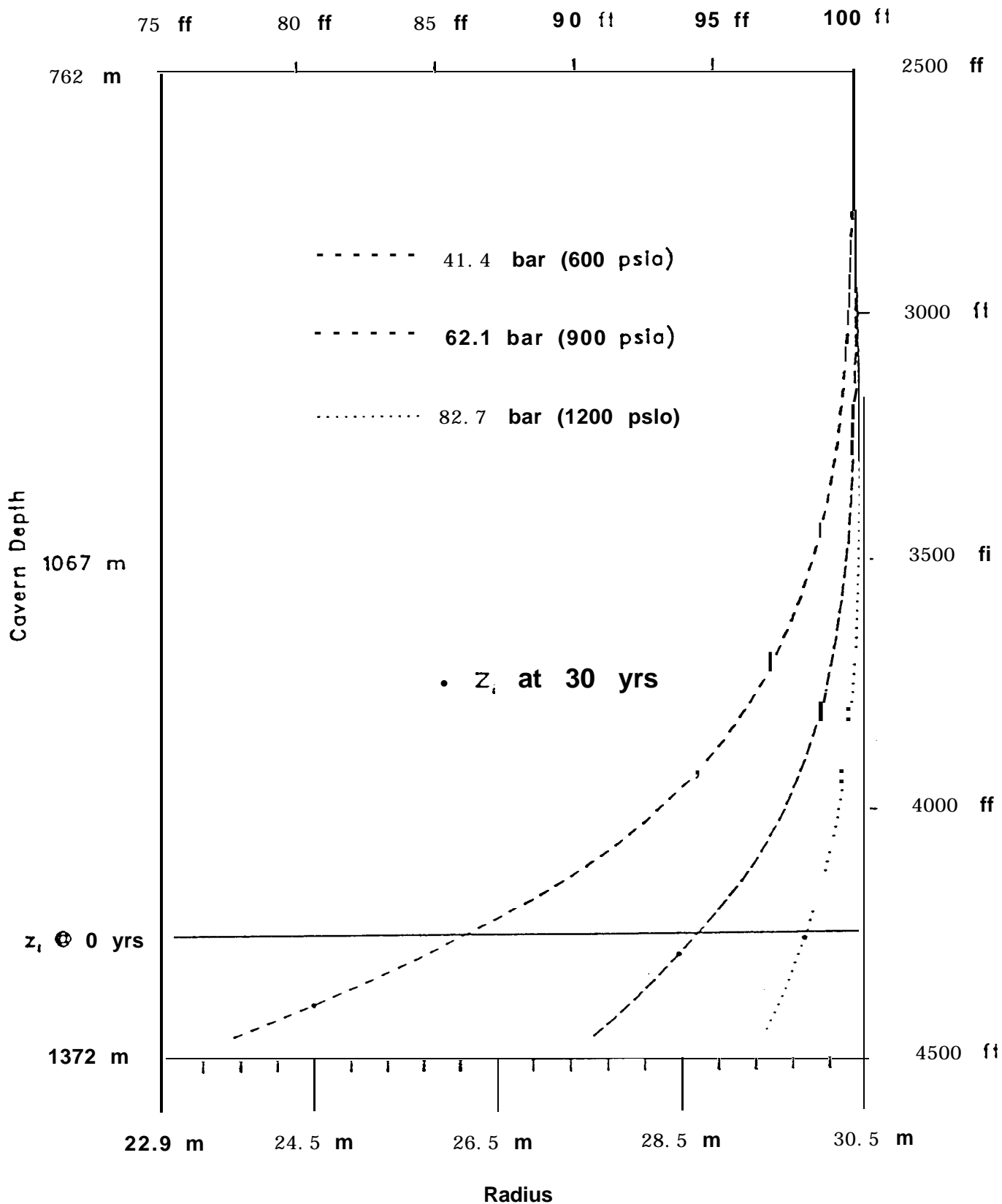
19

Figure 6. Radial profile, r(z), for a 762 m - 1372 m (2500 ft - 4500 ft)
operated for 30 years at 41.4, 62.1, and 82.7 bar (600, 900, and 1200 psia).
The solid horizontal line denotes the initial interface depth, 1295 m
(4250 ft), while the filled black circles on the radial profiles represent the
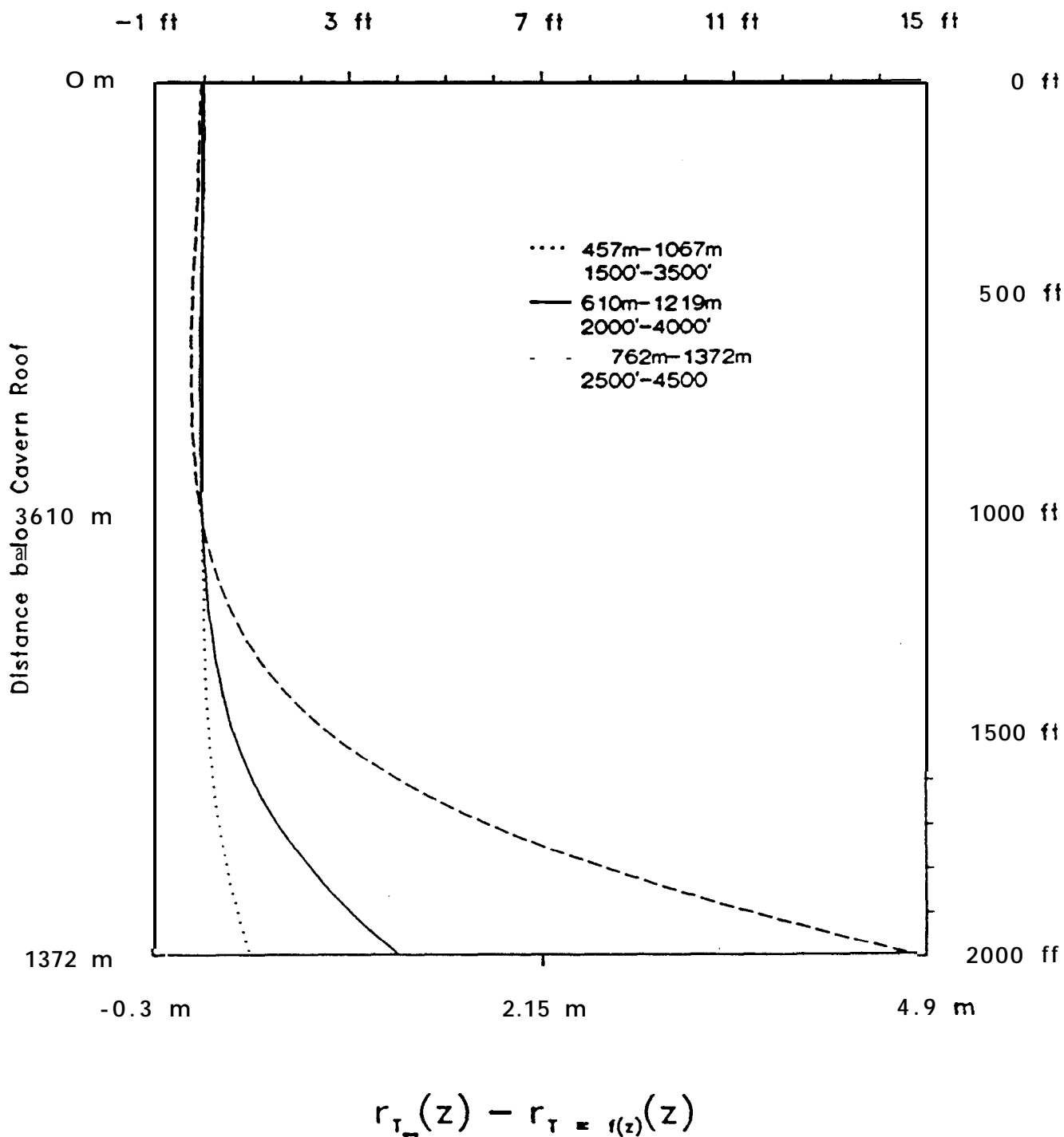interface depth at 30 years.

Figure 7. The difference in the radial profiles as calculated using a linear temperature profile and a average temperature approximation. The three caverns are shown: 457 m - 1067 m (1500 ft - 3500 ft), 610 m - 1219 m (2000 ft - 4000 ft), and 762 m - 1372 m (2500 ft - 4500 ft).

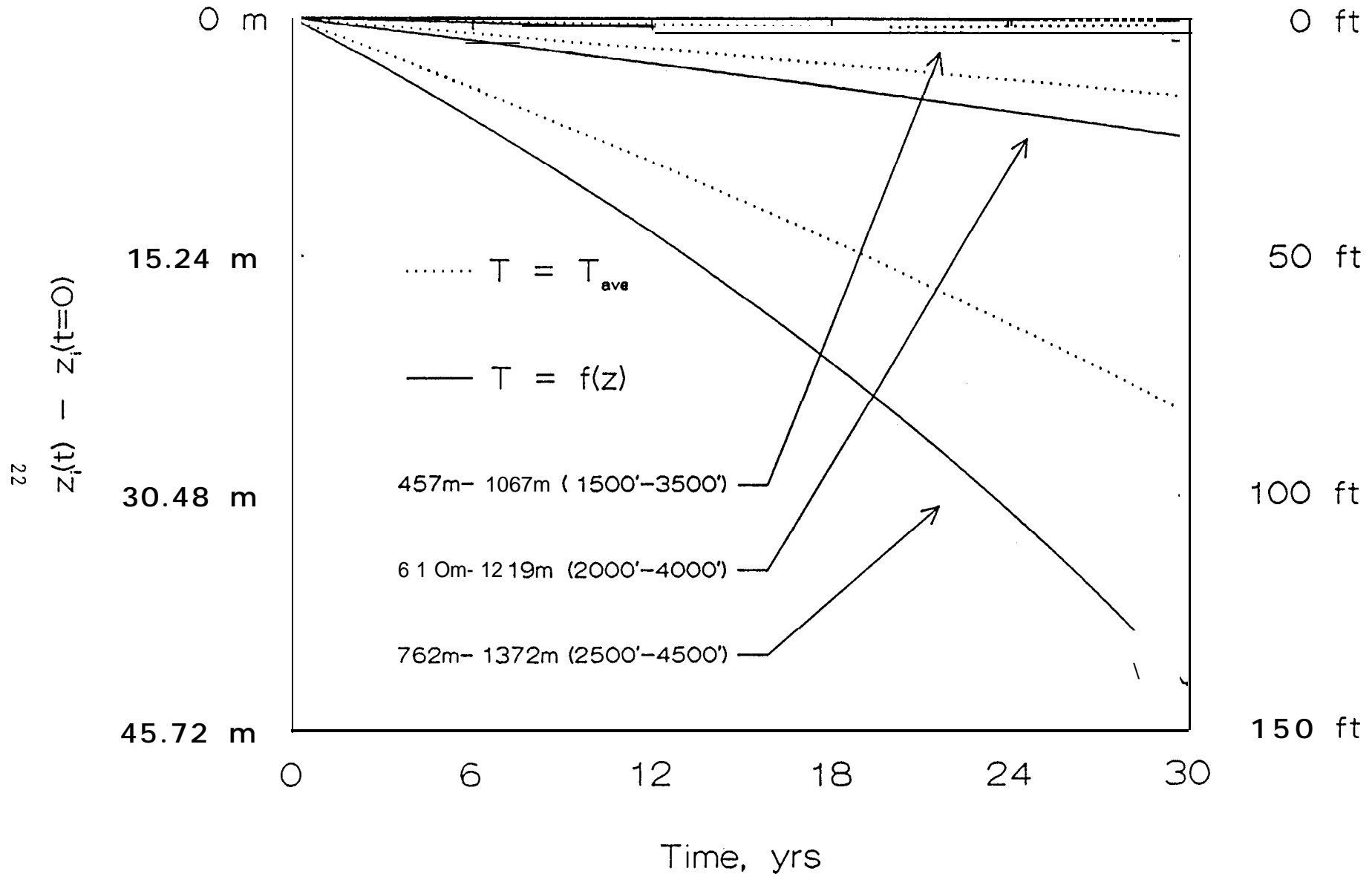# Interface Movement for Three Depths

Figure 8. Interface movement as a function of time, calculated for both the linear temperature profile (solid line) and the average temperature approximation (dotted line). The three caverns shown: 457 m - 1067 m (1500 ft - 3500 ft), 610 m - 1219 m (2000 ft - 4000 ft), and 762 m - 1372 m (2500 ft - 4500 ft), were operated for 30 years at 41.4 bar (600 psia) for 30 years.

percent volume loss for a 610 m (2000 ft) cavern operated for 30 years at a constant P_w = 41.4 bars (600 psia) has been calculated using both temperature profiles for caverns of varying depth and is plotted in Figure 9. Again, we see from this figure that the volume loss predicted by average temperature approximation is less than that predicted by the linear temperature profile and that this deviation increases with increasing cavern depth.

As discussed above, the actual temperature profile in the salt, undoubtedly at least two-dimensional and time dependent, has not been measured. However, the two methods of modelling the temperature profile used in this work provide upper and lower bounds on the actual temperature distribution. Therefore, the actual radial profiles, brine removal rates, and volume losses would be expected to fall somewhere between the results predicted by the two models.

The effect of cavern depth on volume loss for caverns maintained at the same wellhead pressure can also be seen from Figure 9. As discussed above, deeper caverns not only lose more volume to creep, but the relationship between cavern depth and volume loss is not linear. Another commonly discussed issue is where the volume loss occurs in a cavern. This can be determined from the radial profiles generated by this model. The easiest way of characterizing the volume loss distribution is *to* determine percent of the total creep volume loss over the 30 year lifespan as a function of depth. This has been plotted in Figure 10 for the three caverns of varying depth, all operated for 30 years at P_w = 41.4 bars (600 psia). From this figure we can see that for 610 m (2000 ft) caverns operated at P_w = 41.4 bars (600 psia), 80-90% of the volume lost occurs in the bottom 183 m (600 ft) or 30 % of the cavern. In addition, placing the caverns shallower in the dome has the effect of concentrating the volume loss closer to the bottom of the cavern. In other words, the volume loss is less axially distributed in shallow caverns than in deep cavern.

CONCLUSIONS AND FUTURE WORK

Cost considerations require the mitigation of volume loss in SPR caverns whenever possible. Volume loss can be reduced by operating the cavern at a higher wellhead pressure. The percent of the cavern volume saved by increasing the operating pressure a given amount increases with cavern depth. Thus the cost savings of operating SPR caverns at higher wellhead pressures increases with cavern depth. The distribution of the volume loss was found to vary little with cavern depth, with 80-90% of the volume loss occuring in the bottom 30% of the caverns. The two different methods of approximating temperature, using an average temperature and using an axially linear, radially and time invariant temperature profile were found to differ by up to 35% in volume loss prediction with the greater differences occuring at the greater cavern depths.

Volume Loss for Caverns of Varying Depth
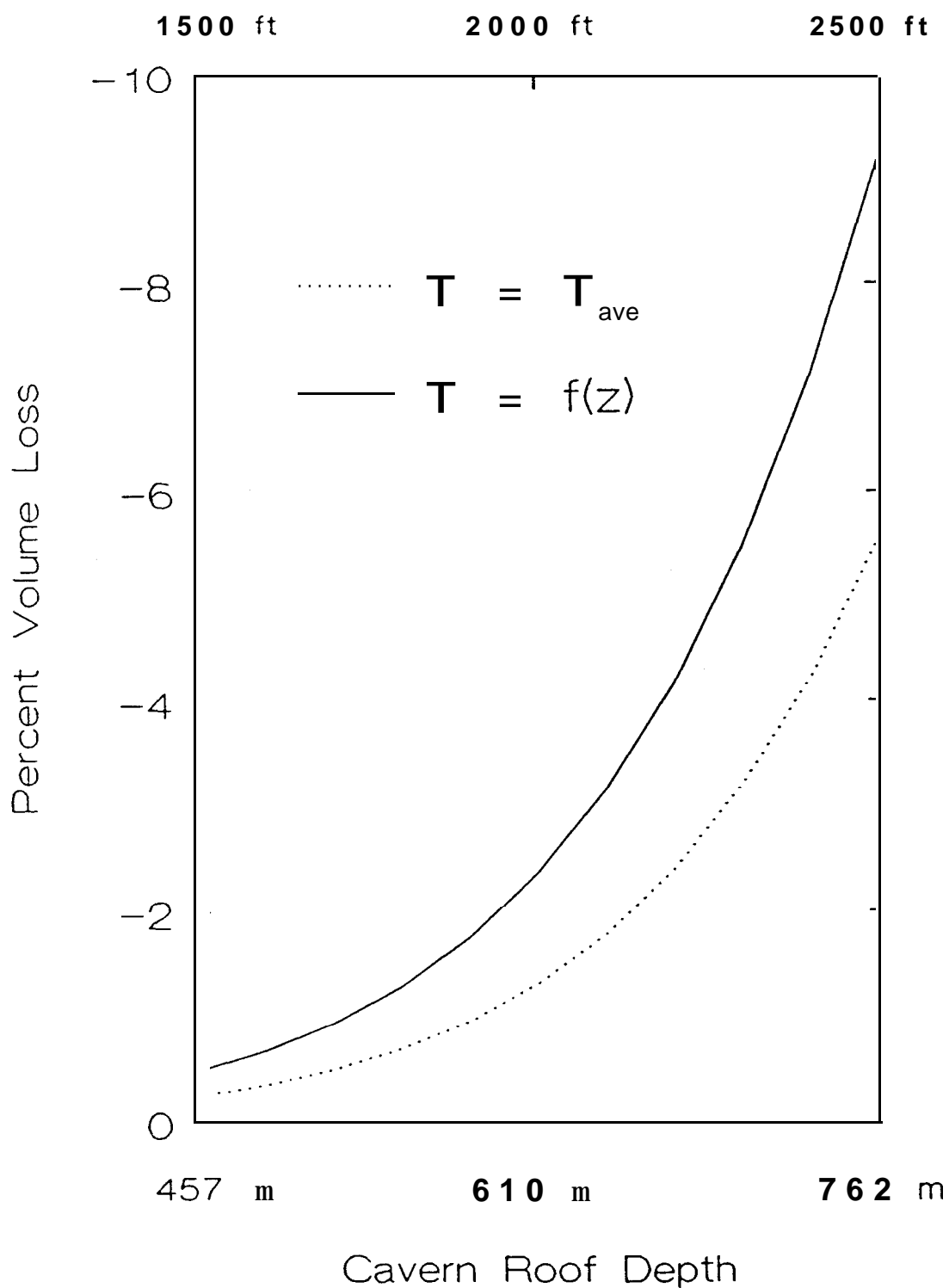
Figure 9. Percent volume loss as *a* function of cavern roof depth for 610 m (2000 ft) caverns operated for 30 years at 41.4 bar (600 psia). The results are shown for both temperature profile models.

Creep Volume Loss:
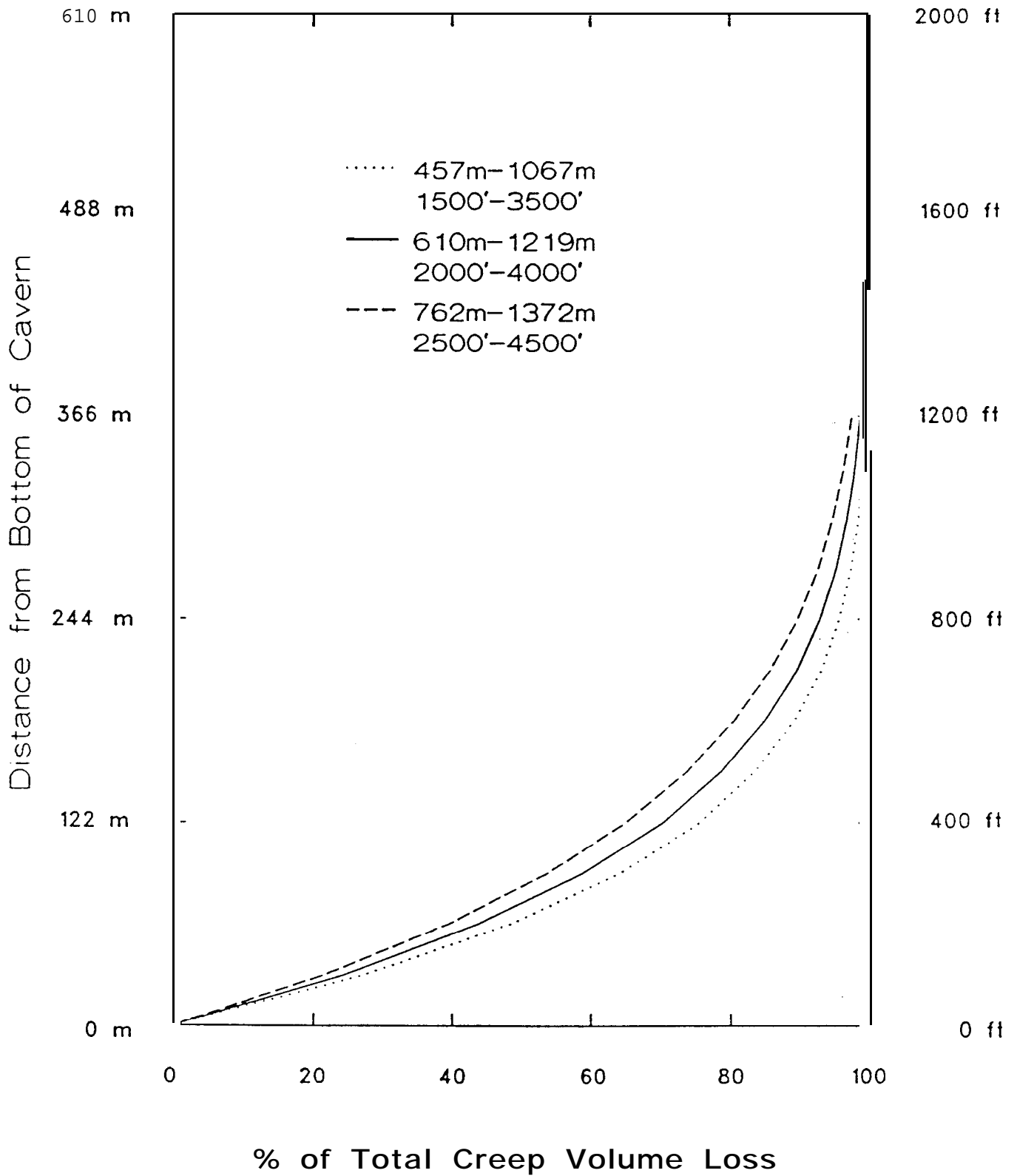## Distribution with Depth

Figure 10. Distribution of volume loss for three caverns: 457 m - 1067 m (1500 ft - 3500 ft), 610 m - 1219 m (2000 ft - 4000 ft), and 762 m - 1372 m (2500 ft - 4500 ft), operated for years at 41.4 bar (600 psia).

Appendix A

Brine Equation of State

As discussed in the text, the model used in this work employs an equation of state for saturated brine. This equation, developed by Todd[24], was developed as follows. Todd's analysis begins with Potter and Brown's[25] equation for brine density as a function of pure water density, temperature, and molality. This equation is based on an interpolation of data available in the literature. By substituting expressions for pure water density and saturated brine molality as functions of temperature and pressure into this equation, Todd developed a complete saturated brine equation of state.

The first of these expressions, pure water density as a function of temperature and pressure, was obtained by curve-fitting data for pure water density as a function of temperature and pressure[26]. The equation for saturated brine molality was more difficult to develop. By fitting data (at 25°C) for the molality of saturated brine published in an older edition of the Handbook of Chemistry and Physics[27] an equation for molality as a function of temperature was obtained. Then, since data on the effect of pressure on solubility at temperatures other than 25°C was unavailable, data reported by Kaufman[28] which gave the rate of change of saturation molality with pressure as 2.0188e-4 per atmosphere, was used to add pressure dependence. Since the pressure effect was small and the temperature range of Brown and Potter's equation was narrow, 0 to 80°C, Todd assumed that the rate of change of molality with pressure to be constant and therefore modified the equation for saturated brine molality as a function of temperature from the Handbook of Chemistry and Physics data to include pressure dependency.

Once these expressions for the density of pure water and the molality of saturated brine, both as functions of temperature and pressure were developed, they were inserted into Potter and Brown's equation for the density of brine as a function of molality and the density of pure water. The final result was the equation of state for brine used in this work.

Appendix B

Creep Model for a Cylindrical Cavern

Van Sambeek[21] has derived an equation for creep in an infinite borehole:

$$\frac{\Delta r}{r \Delta t} = - C \, \exp\left(\frac{- Q}{R_g T}\right) \left(\frac{3}{4}\right)^{(n+1)/2} \left\{\frac{\left|K_{litho} \, z - P(z)\right|}{\mu}\right\} \tag{41}$$

For caverns of large radius, the inward radial creep of the salt surrounding the cavern is small relative to the cavern radius itself. Thus a creep model which is not dependent on the time varying radius of the cavern, but rather the initial radius, can be used. In this appendix this approximation, as applied in this work, is quantified.

From equation (41), it is seen that excepting the r in the denominator of the left hand side, appropriate adjustment of parameters (and keeping n constant) will collapse Van Sambeek's equation to the model used in this work (equation (32):

$$\Delta r = R \, A \, \Delta t \, \exp\left(\frac{- E}{R_g T}\right) \left\{\frac{\left|K_{litho} \, z - P(z)\right|}{\mu}\right\}^{5.5} \tag{42}$$

In an effort to quantify the differences in calculated cavern creep using Van Sambeek's model as opposed to the model used in this work, a comparision study was performed. In this study, four caverns were studied:

Cavern Number	Cavern Depth	Wellhead Pressure	Temperature Model
Cavern 1	610 m - 1219 m (2000 ft - 4000 ft)	41.4 bar (600 psia)	linear
Cavern 2	610 m - 1219 m (2000 ft - 4000 ft)	41.4 bar (600 psia)	average
Cavern 3	762 m - 1372 m (2500 ft - 4500 ft)	34.5 bar (500 psia)	linear
Cavern 4	**762 m - 1372 m (2500 ft - 4500 ft)**	**41.4 bar (600 psia)**	**average**

These caverns were chosen for the following reasons. Caverns 1 and 2 represent "nominal" caverns. These caverns, identical except for the temperature model, are at the depth and operating pressure widely used in the SPR for calculating nominal cavern properties. Cavern 3 represents the deepest cavern and lowest operating pressure studied using the creep model employed in this work. Because this model will deviate from Van Sambeek's model with greater creep, this cavern was investigated to determine the differences between the two models in this regime of greatest deviation. Finally, Cavern 4 is the deepest cavern with the lowest operating pressure investigated in this work with the average temperature approximation. By performing a similar calculation using Van Sambeek's model, the regime of greatest deviation between Van Sambeek's model and the creep model employed in this work with the average temperature approximation can be investigated.

This study was carried out as follows. In order to determine the effect of having the r term in the denominator of equation (41), equation (42) was modified to:

$$
Ar = r \, A \, \Delta t \, \exp\left(\frac{-E}{R_g T}\right) \left\{ \left| \frac{K_{litho} \; z - P(z)}{\mu} \right| \right\}^{5.5} \tag{43}
$$

The proper way of developing a model with Van Sambeek's formulation would have been to collapse the constants in equation (41) to resemble the format of equation (42) and then refit to the actual cavern data used in the development of the present model. However, in the interest of demonstrating that the difference between the models is insignificant, the same constants were used in both cases. That is, the only modification to the present model, including the values of the constants used, was to replace the nominal initial radius R in equation (42) with the actual time-varying radius r. Two parameters were studied, AV and

$r(z_b)$, the volume change and radius at the bottom of the cavern, both at 30 years. The results of this study are tabulated below.

Cavern	Percent Difference Between The Two Creep Models	
	AV (30 yrs)	$r(z_b,\ 30\ \text{yrs})$
Cavern 1	1.5	0.4
Cavern 2	0.8	0.03
Cavern 3	7.4	6.4
Cavern 4	2.6	0.5

As expected, the difference between the two models is greatest for the deepest cavern with the lowest operating pressure, Cavern 3. Interestingly, using the average temperature approximation improves the correlation between the two models.

REFERENCES

1. W. Herrmann, W. R. Wawersik, and S. T. Montgomery, 'Review of Creep Modelling for Rock Salt,' Mechanics of Engineering Materials, Eds. C. S. Desai and S. T. Gallagher, Chapt. 15, John Wiley & Sons Ltd (1984).

2. W. R. Wawersik and D. H. Zeuch, 'Creep and Creep Modelling of Three Domal Salts --A Comprehensive Update,' Sandia Laboratories Report SAND84-0568 (1984).

3. 'Rock Mechanics Models Evaluation Report,' Fluor Technology, Inc DOE/CH/46656-09 (1987).

4. P. E. Senseny, 'Review of Constitutive Laws Used to Describe the Creep of Salt,' Office of Nuclear Waste Isolation, Battelle Memorial Institute ONWI-295 (1983).

5. P. C. Kelsall and J. W. Nelson, *Geologic and Engineering Characteristics of Gulf Region Salt Domes Applied to Underground Storage and Mining,' proceedings Sixth International Symposium on Salt, Northern Ohio Geological Society, 519-544 (1983).

6. H. S. Morgan, C. M. Stone and R. D. Krieg, 'The Use of Field Data to Evaluate and Improve Drift Response Models for the Waste Isolation Pilot Plant (WIPP),' Proceedings of 26th U.S. Symposium on Rock Mechanics, (1985).

7. C. A. Anderson, 'An Investigation of the Steady Creep of a Spherical Cavity in a Half Space,' Transactions of the ASME, June (1976).

8. L. L. Van Sambeek, 'A Simple Method for Modelling the Pressure Buildup or Flow of an Abandoned Solution Well,' presented at Solution Mining Research Institute Meeting, Austin, Texas (1990).

9. D. S. Preece, R. R. Beasley and K. L. Goin, 'Borehole Creep Closure Measurements and Numerical Calculations at the Big Hill Texas SPR Storage Site,' Sandia Laboratories Report SAND86-0876C (1986).

10. D. S. Preece and J. T. Foley, 'Finite Element Analysis of Salt Caverns Employed in the Strategic Petroleum Reserve,' proceedings, Sixth International Symposium on Salt, Northern Ohio Geological Society, 49-63 (1983).

11. A. J. Russo, 'A Solution Mining Code for Studying Axisummetric Salt Cavern Formation,' Sandia Laboratories Report SAND81-1231 (1981).

12. J. L. Ratigan and K. L. DeVries, 'Potential Geomechanics Problems Resulting from Closely Spaced Storage Wells in Dome Salt,' SPE Gas Technology Symposium, Proceedings, Society of Petroleum Engineers of AIME, 279-286 (1989).

13. F. J. Fischer, 'An Axisymetric Method for Analyzing Cavity Arrays,' proceedings, <u>First Conference **on the** Mechanical Behavior</u> of <u>Salt</u>, Trans Tech Publications, 661-679 (1981).

14. J. L. Todd, 'An Evaluation of SPR Cavern Operation at Low Pressure,' <u>Sandia Laboratories **Report SAND85-0830**</u> (1985).

15. G. S. Heffelfinger, 'The Usefulness of Interface Depth Measurements in Determining the Existence of Leaks in SPR Caverns,' <u>Sandia Laboratories Report,</u> in preparation (1991).

16. S. W. Webb, 'Calculation of Transient Fluid Velocities in SPR Caverns,' <u>Sandia Laboratories **Report**,</u> in preparation (1990).

17. D. Tomasko, 'Preliminary SPR Thermal Model Description and Results for **WH-**11 and BM-4,' <u>Sandia Laboratories **Report**</u>, **SAND84-1957** (1984).

18. <u>Petroleum Production Handbook,</u> Eds. T. C. **Frick** and R. W. Taylor, Society of *Petroleum* Engineers of AIME (1962).

19. <u>Handbook</u> of <u>Chemistry **and** Phvsics.</u> 59th Edition, Eds. R. C. Weast and M. J. **Astle,** CRC Press (1978).

20. W. E. Boyce and R. C. **DiPrima,** <u>Elementary Differential Equations **and** Boundary Value Problems</u>, **3ʳᵈ** Edition, John Wiley **&** Sons, New York, 1977.

21. L. L. Van Sambeek, 'Creep of Rock Salt under Inhomogeneous Stress Conditions,' Ph. D. Thesis, Colorado School of Mines, Golden, CO. (1986).

22. D. S. **Preece** and R. D. Krieg, 'Application of a Continuum Model to Predict Creep Closure of Cavities in Rock Salt,' <u> Transactions</u>, <u>American Geophysical Union</u>, Vol. 64, No. 45, p. 840, (1983).

23. M. P. Allen and D. J. Tildesley, <u>Computer Simulation</u> of <u>Liauids</u>, Clarendon, 1987.

24. J. L. Todd, Sandia National Laboratories, memorandum to J. K. Linn dated September 19, 1989.

25. R. W. Potter and D. L. Brown, 'The Volumetric Properties of Aqueous Sodium Chloride Solutions from 0°C to 500°C at Pressures Up to 2000 Bars Based on a Regression of Available Data in the Literature, Geological Survey Bulletin 1421-C (1954).

26. <u>American Institute</u> of <u>Phvsics Handbook</u>, 2nd Edition, McGraw-Hill, New York (1963).

27. <u> Handbook</u> of <u>Chemistrv **and** Physics,</u> 30th Edition, CRC Press, Cleveland (1948).

28. D. W. Kaufman, 'Sodium Chloride,' ACS Monograph 145, Hafner Publishing Co, New York (1968).

Distribution:

US DOE SPR **PMO** (4)
900 Commerce Road East
New Orleans, LA 70123
Attn: TDCS (2)
            E. E. Chapple
            D. W. Whittington

USDOE SPR **PMO** (2)
1000 Independence Avenue SW
Washington, DC 20585
Attn: D. Johnson
            D. Smith

Boeing Petroleum Services, Inc. (3)
850 S. Clearview Parkway
New Orleans, LA 70123
            K. E. Mills
            K. D. Wynn
            T. Eyermann

6000   V. L. Dugan
6200   B. W. Marshall
6250   P. J. Hommert
6253   D. S. **Preece**
6257   J. K. Linn (10)
6257   G. S. Heffelfinger (10)
6257   J. T. Neal
6257   J. L. Todd
6257   B. L. Ehgartner
6257   P. S. Kuhlman
1514   H. S. Morgan
3141   S. Landenburger (5)
3151   G. C. **Claycomb**
            For DOE/TIC (Specified External
                    Distribution Only)
8523   R. C. Christman (Library)